Patch Antenna System for CubeSats in L band

Miroslav J. Veljovic, Anja K. Skrivervik
Microwave and Antenna Group (MAG), Ecole Polytechnique Fédérale de Lausanne, Switzerland, miroslav.veljovic@epfl.ch

***Abstract*—An L-band patch-antenna system for CubeSat applications is presented in this paper. The high-permittivity dielectric loading reduces the size of individual antennas to make them suitable for a CubeSat platform. Two circularly polarized patch antennas were designed for the downlink and uplink frequencies of 1.53 and 1.63 GHz, respectively, and the antenna prototypes were characterized. A two-element, sequentially rotated antenna array was designed using the uplink patch element at 1.63 GHz, with a beam tilt of 20° from broadside. The array is to be employed in a system of four arrays that provide two tilted beams with dual-band coverage in each beam, for an increased system capacity. The arrays are located on the backside of the 3U-CubeSat solar panels, facing Earth. While the panels are stowed, the antennas of two arrays are interleaved, reducing the required stowage volume.**

***Index Terms*—patch antenna, antenna array, CubeSat, beam, solar panel.**

I. Introduction

CubeSat is the most popular nanosatellite standard [1]. Since it appeared as an academic student project, the CubeSat standard demonstrated it's potential in the space industry as well, due to its low development and deployment cost. Over eight hundred CubeSats were launched, a majority of which by companies [2], and entire constellations are envisioned in the future.

Each CubeSat weighs several kilograms and is made of 100x100x100 mm^2 cubes, called Units. The three-Unit (3U) is currently the most frequent form factor among CubeSats [2]. The CubeSats onboard power is partially supplied through solar panels placed on the satellite surface and the deployable wings. Each wing can have a total surface of up to 300 x 300 mm2, which corresponds to three long faces of a 3U CubeSat [3].

A majority of the commercial CubeSats is placed in the Low Earth Orbit (LEO). A short orbital period in LEO limits the time of visibility between the CubeSat and a fixed point on the ground. The CubeSat antennas should therefore possess a wide beamwidth to maximize the link duration. The early CubeSats typically communicated via dipole antennas in the UHF band, due to good propagation characteristics and the availability of system components at those frequencies [4]. Over time, attitude determination and control systems (ADCS) became available for CubeSats [5]. This led to the use of higher-gain antenna geometries, typically patch antennas. Patch antennas operate at higher frequencies, providing larger bitrates, and their low profile allows placement on the satellite surface.

CubeSats can benefit from the frequency bands allocated for the legacy space-communication networks in L band (Iridium, GlobalStar) [6]. However, the wavelength at those frequencies is still considerable (200 mm @ 1.5 GHz), compared with the CubeSat size. Therefore, various miniaturization techniques must be applied during the antenna design in order to fit the antennas on a CubeSat face. Additionally, the antennas can be placed on the Earth-facing sides of the solar panels. The ground plane below the solar cells can then serve as the ground for the antennas placed on the opposite side of the panel.

A variety of low-profile antennas was proposed and studied in the literature. In [7], it was shown that the impedance and radiation properties of low-profile antennas are strongly dependent on their placement onboard small satellites. A two-element array of dual-linearly polarized meshed patches, described in [8], uses sequential rotation for a wideband axial-ratio performance.

In this paper, we present a design procedure for a CubeSat circularly polarized (CP) patch-antenna system operating in L band. The downlink (DL) and uplink (UL) frequencies of 1.53 and 1.63 GHz, respectively, are allocated for mobile satellite services by the ITU [9]. A heavy dielectric loading reduces the size of individual CP antennas, and enables the use of small arrays onboard. Two DL and two UL patch antenna arrays, located on the back of the solar-panel wings, each exhibit a 45° x 90° beamwidth, with a beam tilt of 20°. The inherent radiation pattern distortion, due to an asymmetric ground plane, is used here to our advantage to improve the radiation in the tilted beams. The antenna system provides two tilted beams, with a duplex communication in each beam, as a means of system capacity increase. A convenient antenna configuration is proposed, which minimizes the stowed volume of the solar panels, by interleaving the antennas of the two arrays, located on the adjacent wing panels.

II. Circularly Polarized Patch Antennas

A. Antenna Geometry

The elements of the antenna arrays are considered first. Two CP patch antennas were designed for the operation at 1.53 (DL) – transmit (Tx) antenna and 1.63 GHz (UL) – receive (Rx) antenna. Square patches with chamfered corners are printed on a high-permittivity low-loss dielectric substrate Rogers TMM10i (ε_r=9.9, tan δ=0.002, h=5.08 mm) which has stable electrical characteristics in a large temperature range. The high permittivity dielectric significantly reduces the antenna size. Consequently, the impedance bandwidth is also reduced, and a large substrate thickness was selected to alleviate this effect. During the analysis, the antennas were placed on a 100x300 mm^2

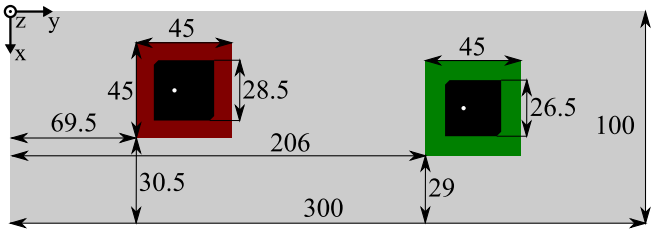

Fig. 1. Patch antennas on a 3U-CubeSat solar-panel wing (units in mm).

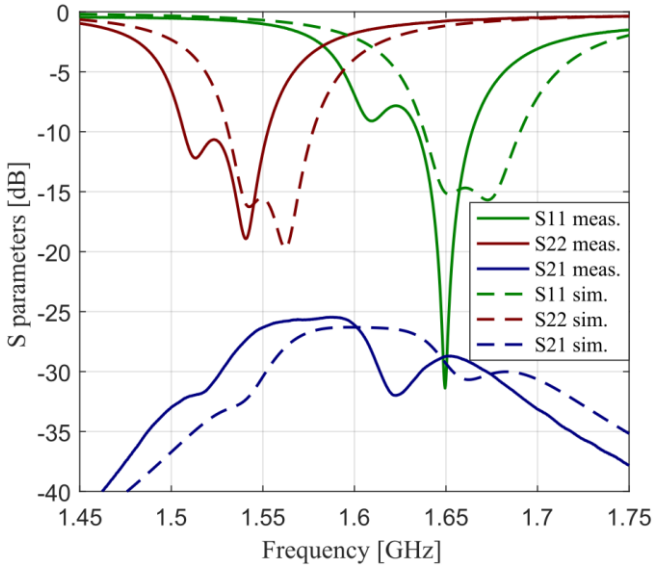

Fig. 2. Measured and simulated S parameters of the antennas from Fig. 1.

metallic panel, as shown in Fig. 1, to model a solar-panel wing of a 3U CubeSat. The antenna placement was arbitrary in order to evaluate the influence it has on the matching and the radiation pattern.

B. Simulation and Measurement Results

Antenna prototypes were fabricated and placed on a metallized 100x300-mm^2 FR4 panel for anechoic chamber measurements, similarly as during the simulations (Fig. 1). The antennas are fed using a small MMCX connector with a lock-snap mechanism. After the first set of prototypes was characterized, a frequency shift of ~0.035 GHz was observed in the measured S parameters, as compared to the simulations. The discrepancy was attributed to the connectors, which were not included in the simulation model, and an inaccurate estimation of the dielectric permittivity. The frequency shift is compensated in the second set of prototypes, for which the antennas were designed at an appropriately higher frequency. Measured S parameters are compared with the simulated ones in Fig. 2. Realized gain and AR values of both prototypes are presented in Fig. 3. The gain of the Rx antenna is lower due to a mismatch caused by the used connector. The measured and simulated radiation patterns are shown in Fig. 4, only for the Rx antenna, as the Tx antenna has a similar performance.

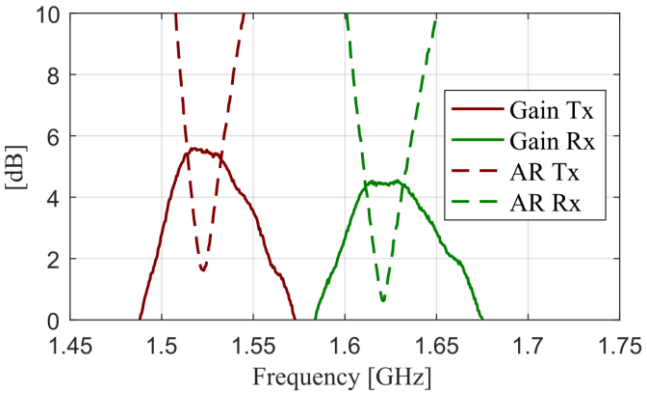

Fig. 3. Measured gain and axial ratio of the antennas from Fig. 1.

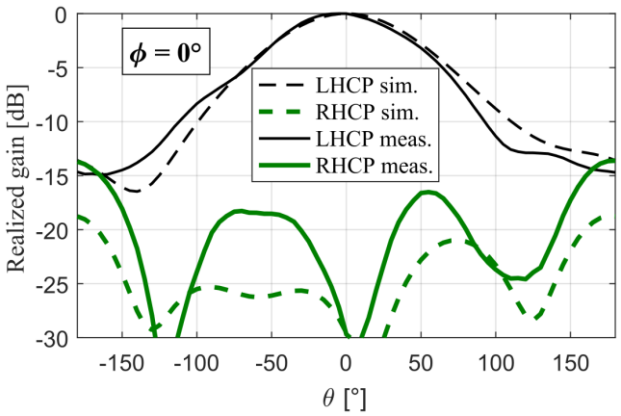

(a)

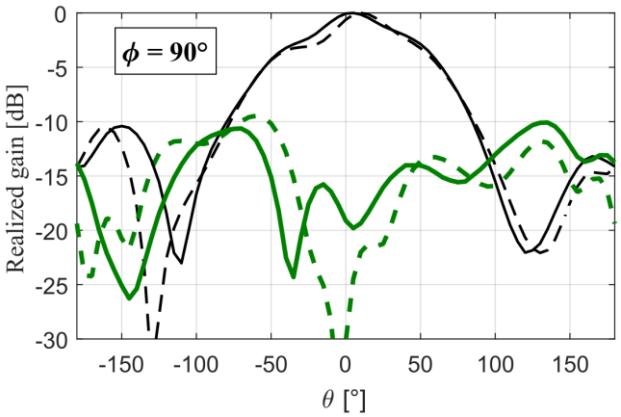

(b)

Fig. 4. Measured and simulated radiation patterns of the UL (green) antenna from Fig. 1. (a) φ=0°. (b) φ=90°.

The patches exhibit a wide beamwidth of ~90°, conforming to the design requirements. The radiation results show that the patterns in the φ=0° plane are not influenced by the antenna offset with respect to the long axis of the satellite face, except for a small beam tilt of 5°. However, there is a significant pattern distortion in the φ=90° plane as a consequence of a large ground. This effect has an adverse effect on the radiation when used in an array, which will be explained in the following sections.

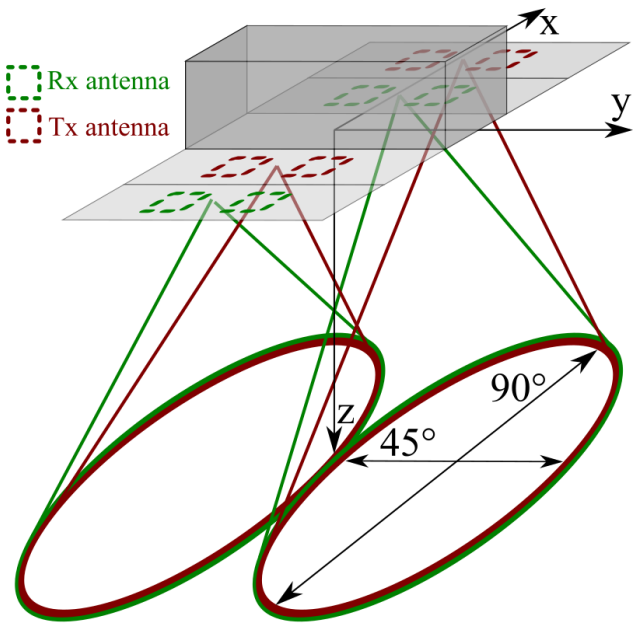

Fig. 5. A visual representation of two tilted beams, served by four 2x1 patch arrays.

III. Circularly Polarized Antenna Arrays

A. Radiation Beams

To increase the capacity of the CubeSat communication system, several independent beams can be employed to cover subsections of the total coverage area. A full duplex functionality requires each beam to include both Tx and Rx frequencies. Here we will consider a scenario of having two 90° x 45° beams, each with a beam tilt away from the broadside. An illustration of this scenario is shown in Fig. 5.

B. Two-Element Antenna Array

Without loss of generality, the scenario can be analyzed considering only one frequency, 1.63 GHz. The Rx patch antenna, described in the previous section, is used to create two-element arrays, and the inter-element spacing is tuned to provide the required beamwidth in the narrow plane. A two-element CP array is shown in Fig. 6. The array center coincides with the wing center. The inter-element spacing of 100 mm yields a beamwidth of 45°, and the beam tilt of -22° is enabled by an appropriate relative phase shift.

Sequential rotation of the two elements can be used to improve the axial ratio performance in both frequency and angular coverage. This technique was tested on the array shown in Fig. 6, where the elements' rotation angles α and β take values of 0, 90, 180 or 270°. The antenna ports were excited differently depending on the rotation angle, to obtain a 22.5° beam tilt. Active-S parameters were calculated at each port, which take into account both the matching and the cross coupling between elements. The array was analyzed in various element configurations, and the results of two representative examples are presented in the following sections.

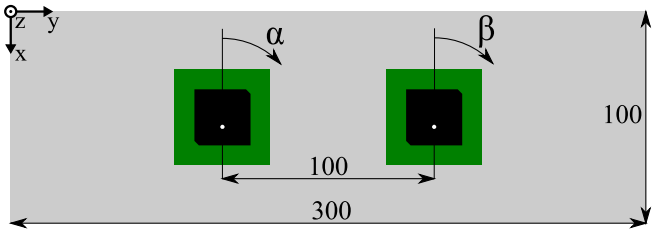

Fig. 6. A 2x1-array of Rx patch elements (units in mm). The rotation angles of left and right elemets are denoted with α and β, and the remaining dimensions are the same as in Fig. 1.

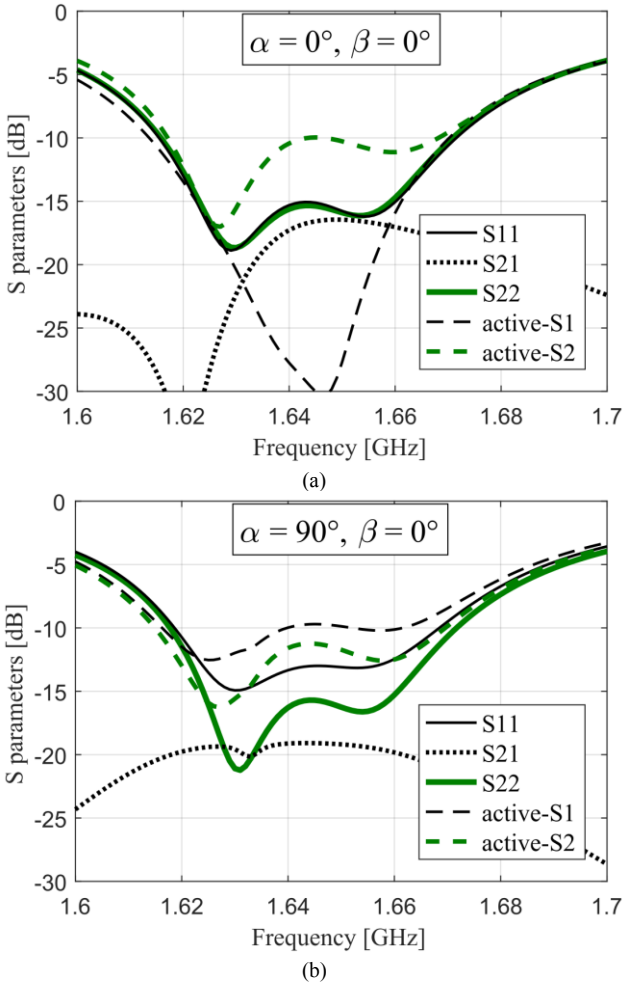

Fig. 7. S parameters of the array from Fig. 6, for various rotation angles α and β. (a) α=0°, β=0°, (b) α=90°, β=0°.

C. S parameters

The simulated S parameters for the two combinations of rotation angles are shown in Fig. 7. It was observed that the S_{11} parameter depends on the antenna position and the rotation angle. The individual antenna elements can be further adapted for each rotation angle, but it was avoided here for simplicity. The characteristic active-S parameter values demonstrate the influence of the mutual coupling on the antenna matching. Through the analysis, this effect varied with the change of the rotation angle and the applied

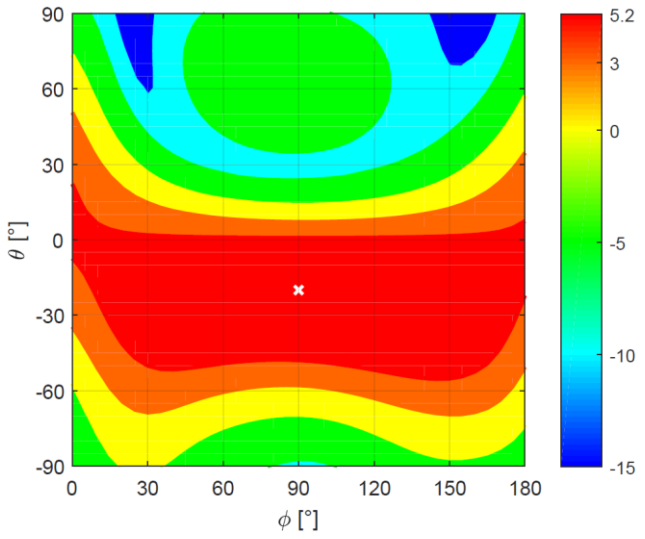

(a)

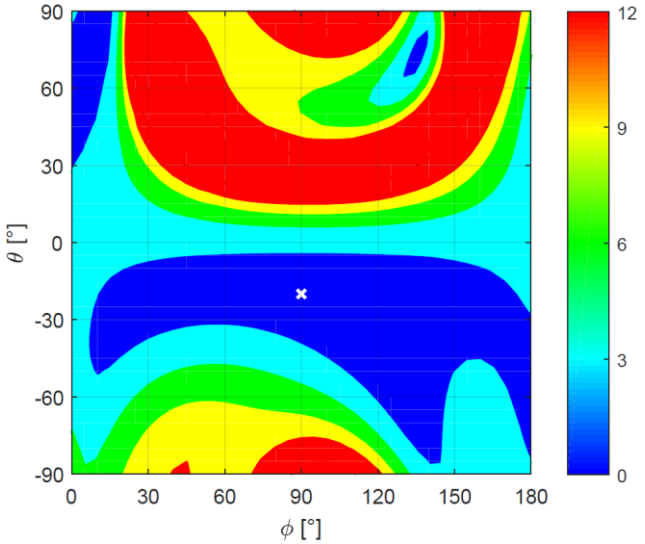

(b)

Fig. 8. (a) The directivity and (b) axial ratio of the array from Fig. 6, versus spherical angles, with a beam tilt of -20°.

phase shift. If the elements are equally oriented (Fig. 7(a)), the active-S_1 parameter is improved. On the other side, both active-S parameters deteriorate in case of a 90° relative rotation, as seen in Fig. 7(b). Despite the effect, the S-parameters of both antennas remain below -10 dB for all analyzed scenarios.

D. Radiation Performance

The AR and directivity of an array with α=90° and β=0° are calculated at 1.63 GHz and the results are presented in Fig. 8 versus spherical angles. The array maintains a similar beamwidth for φ values between 25° and 170°. The AR values do not exceed 6 dB across the array beamwidth, and the average value in this range is 2.63 dB.

The AR and realized gain versus frequency, calculated at φ=90° and θ=-20° (the white 'x' marker in Fig. 8), are presented in Fig. 9, for the two scenarios in section II.*C*.

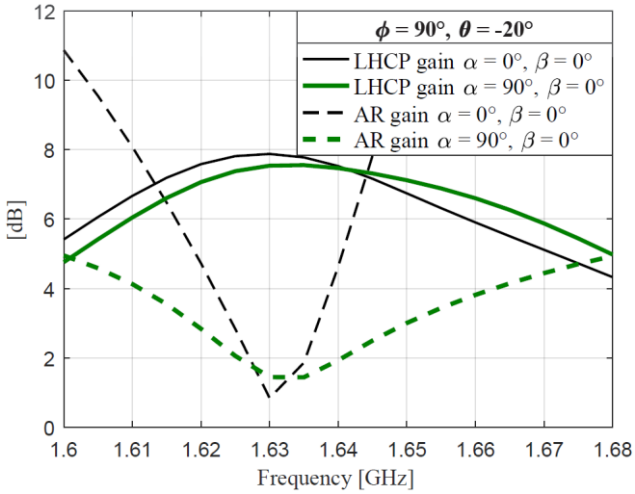

Fig. 9. Realized gain and axial ratio of the array from Fig. 6, versus frequency, for various rotation angles α and β.

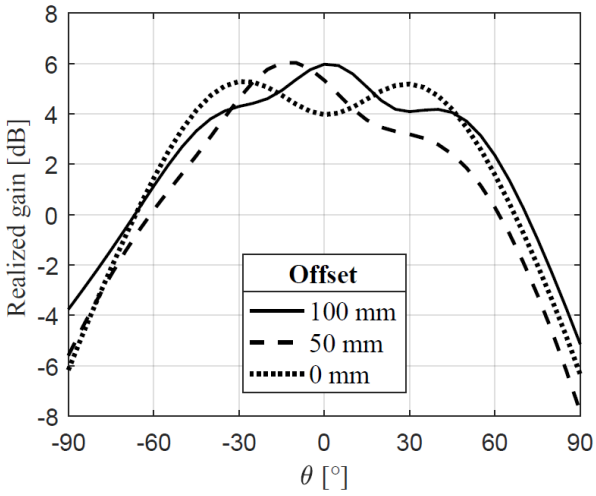

Fig. 10. Realized gain of a patch antenna placed on a 300x100 mm^2 ground plane, for different values of offset from the ground plane center.

The 3-dB gain bandwidth of both models is ~100 MHz (6%). The array with sequential rotation yields AR values smaller than 5 dB along the entire gain bandwidth (3-dB bandwidth of 1.9%), a considerable improvement over the non-rotated model (3-dB bandwidth of 0.8%).

The radiation patterns of individual elements are similar to the ones shown in Fig. 4, and the gain values of left and right patch elements at φ=90°, θ=-20°, are 5.7 and 3.5 dBi, respectively. Due to this difference, the CP components of the total radiated field are not equal, and the minimum AR value is not smaller than 1.4 dB. The beam tilt is attributed to the radiation of additional electric currents, flowing on the larger part of the ground in the antenna vicinity.

To investigate the effect of pattern distortion, a single element was analyzed on a 300x100-mm2 metallic plane, for various values of offset from the plane center. The resulting realized-gain patterns are presented in Fig. 10. These patterns can be used to assess the total radiation of an array, for an arbitrary antenna placement.

IV. Antenna Array Placement and Stowage

As each of the described antennas operates only in a single frequency band, four antennas per frequency band are required for the two duplex beams. Based on their size, a set of four antennas can fit under a single solar-panel wing. However, they cannot be arbitrarily distributed, as the inter-element distance of each array is fixed. Furthermore, the cross coupling of such configuration would be considerable. A different approach would be to place each two-element antenna array on a separate 3U wing section, as shown in Fig. 11. In this configuration, the wings are folded with the antennas facing each other. If placed properly, the two pairs of antennas are interleaved when stowed, as seen in the top of Fig. 11. This approach minimizes the added thickness that the antennas introduce to the solar wings in their stowed position.

The limiting factor in achieving a better AR performance is an inherent beam distortion in the patterns of individual elements, caused by the antenna placement on the large ground plane. Here, the difference from the previously analyzed array, shown in Fig. 6, is that each of the arrays pictured in Fig. 11 is shifted towards one side of the ground plane. The elements' radiation patterns from Fig. 10 can then be used to predict the radiation of the shifted array, and tilt the beam towards the more favorable direction (+20° or -20°) in terms of gain and AR.

V. Conclusions

This paper investigates the performance of L-band patch antennas and arrays, placed on the backside of 3U CubeSat solar-panel wings. Two CP antenna prototypes, designed at uplink and downlink frequencies, possess a small size and a large beamwidth of 90°, due to a high-permittivity dielectric loading. The patches are employed in a system of four two-element arrays, which provide two 45° x 90° duplex beams for increased capacity, and the uplink array is analyzed here in detail. It is shown that a radiation pattern distortion, caused by a large ground plane, can be used to improve the total array gain in a tilted beam. The measurement results of the antenna array will be presented during the conference.

A method of efficient patch antenna stowage in proposed, where the antennas are placed on separate solar-panel wings and interleaved while the wings are stowed. The total stowed thickness can be further reduced by using a thinner antenna substrate, sacrificing the element bandwidth. The proposed patch arrays can be adapted for other CubeSat scenarios, where only two 3U solar-panel wings are available. In this context, a suitable dual-band antenna element would reduce the total number of required antennas to four.

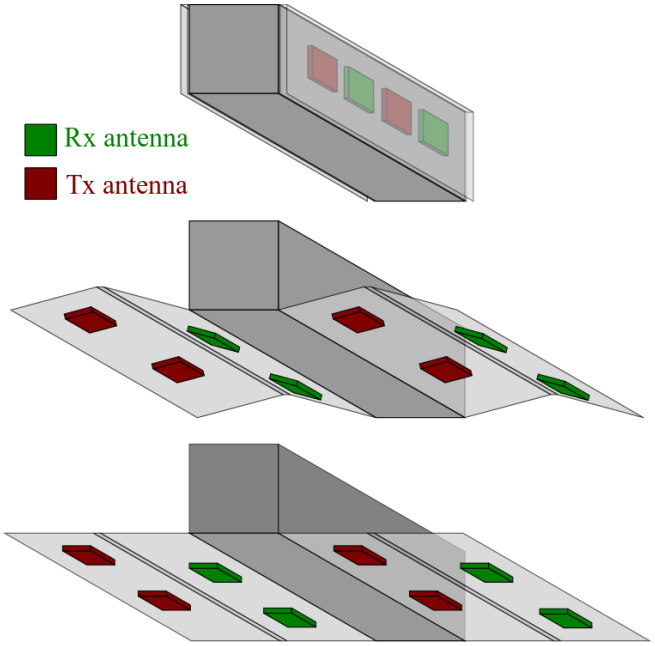

Fig. 11. The deployment procedure of a 3U-CubeSat solar wings, with the proposed configuration of the patch-antenna arrays.

Acknowledgment

This work was funded by the Swiss Commission for Innovation and Technology, in the project 18328.1.

References

[1] S. Lee, A. Hutputanasin, A. Toorian, W. Lan, R. Munakata, J. Carnahan, D. Pignatelli, and A. Mehrparvar, "CubeSat design specification, rev. 13: The CubeSat program," California Polytechnic State Univ., San Luis Obispo, 2014.

[2] E. Kulu, "Nanosatellite database by Erik". Accessed on: September 30, 2018, [Online] Available: http://nanosats.eu/index.html#figures.

[3] Planet Labs, Inc., 2018, [Online] Available: https://www.planet.com/

[4] C. Kakoyiannis and P. Constantinou (April 4th 2011). "Electrically Small Microstrip Antennas Targeting Miniaturized Satellites: the CubeSat Paradigm," in *Microstrip Antennas*, IntechOpen, 2011, DOI: 10.5772/14947.

[5] S. Gao, Y. Rahmat-Samii, R. E. Hodges, and X. X. Yang, "Advanced antennas for small satellites," Proc. IEEE, vol. 106, no. 3, pp. 391–403, 2018.

[6] NASA, "State of the art of small spacecraft technology - communications", 2018, [Online] Available: https://sst-soa.arc.nasa.gov/09-communications.

[7] K. Muchalski et al., "Optimizing TT&C antenna placement on minisatellites," 15th Int. Conf. Microwaves, Radar Wirel. Commun. (IEEE Cat. No.04EX824), vol. 2, 2004.

[8] X. Liu et al., "Transparent and Nontransparent Microstrip Antennas on a CubeSat," IEEE Antennas Propag. Mag., vol. 59, no. 2, pp. 59–68, 2017.

[9] ITU-R Radio Regulations, Edition of 2016, RR5.69, 2016.